



Nanoscale

Membrane-selective Nanoscale Pores in Liposomes by a Synthetically Evolved Peptide: Implications for Triggered Release

Journal:	<i>Nanoscale</i>
Manuscript ID	NR-ART-05-2021-003084.R1
Article Type:	Paper
Date Submitted by the Author:	20-Jun-2021
Complete List of Authors:	Sun, Leisheng; Tulane University School of Medicine, Department of Biochemistry Hristova, Kalina; Johns Hopkins University, Dept Mat Sci/Eng Wimley, William; Tulane University School of Medicine, Department of Biochemistry

SCHOLARONE™
Manuscripts

Membrane-selective Nanoscale Pores in Liposomes by a Synthetically Evolved Peptide: Implications for Triggered Release

Leisheng Sun[†], Kalina Hristova[‡], William C. Wimley^{†*}

[†] Department of Biochemistry and Molecular Biology, Tulane University School of Medicine, New Orleans, Louisiana, 70112, United States. [‡] Department of Materials Science and Engineering and Institute for NanoBioTechnology, Johns Hopkins University, Baltimore, MD, 21218, United States.

AUTHOR INFORMATION

Corresponding Author

William C. Wimley - Department of Biochemistry and Molecular Biology, Tulane University School of Medicine, New Orleans, Louisiana, 70112, United States. Email: wwimley@tulane.edu.

Phone: 504-988-7076

Abstract

Peptides that form nanoscale pores in lipid bilayers have potential applications in triggered release, but only if their selectivity for target synthetic membranes over bystander biomembranes can be optimized. Previously, we identified a novel family of α -helical pore-forming peptides called “macrolittins”, which release macromolecular cargoes from phosphatidylcholine (PC) liposomes at concentrations as low as 1 peptide per 1000 lipids. In this work, we show that macrolittins have no measurable cytolytic activity against multiple human cell types even at high peptide concentration. This unprecedented selectivity for PC liposomes over cell plasma membranes is explained, in part, by the sensitivity of macrolittin activity to physical chemical properties of the bilayer hydrocarbon core. In the presence of cells, macrolittins release all vesicle-entrapped cargoes (proteins and small molecule drugs) which are then readily uptaken up by cells. Triggered release occurs without any direct effect of the peptide on the cells, and without vesicle-vesicle or vesicle-cell interactions.

Introduction

Liposome encapsulation of macromolecular cargoes such as oligonucleotides, antibodies, enzymes, and other therapeutic proteins can improve stability and provide very long circulation time *in vivo*.¹ Further, drug-containing liposomes can accumulate specifically in diseased tissue, including tumors, due to enhanced permeability and retention.² However, spontaneous release of macromolecules can be very slow, thus failing to provide the high drug concentrations at desired locations that are needed for therapeutic effect.³ This has prompted researchers to test liposomes with permeabilities that are sensitive to triggers such as temperature, magnetic field, pH, or light.⁴ Peptide triggered release has not been pursued often because most membrane-permeabilizing peptides also have cytolytic activity and do not release macromolecules, limiting their utility.⁵

An ideal peptide for this application would permeabilize liposomes of a specific lipid composition and release both macromolecule and small molecule cargos, while having no cytolytic activity against cell membranes. In contrast, melittin, the archetypal membrane-permeabilizing peptide from bee venom, has low selectivity. Melittin is a 26-residue peptide that folds into α -helical structure in lipid membranes^{6,7} and permeabilizes many different cell membranes and synthetic bilayers with similar potency. Further, melittin releases small molecules much better than macromolecules.⁸ Towards the goal of creating more useful membrane permeabilizing peptides, we have evolved gain-of-function analogs of melittin in two generations to increase potency, controllability, and membrane selectivity for permeabilization. The first-generation rational combinatorial library of 7,776 members was based on the sequence of melittin. By screening for potent, equilibrium pore-formers, we identified an analog, MelP5, which is much more potent than melittin (**Fig. 1A&S1A**) despite sharing 77% sequence identity. Importantly, MelP5 enables the passage of macromolecules across bilayers at concentrations where melittin and other pore-forming peptides do not.⁹ But MelP5, like melittin, is not strongly membrane selective, and is highly cytolytic against mammalian cells.¹⁰ Subsequently, MelP5 was used as a template for a second-generation library of 18,432 members. In this generation, acidic residues were allowed in six sites with *i* to *i*+3 and *i* to *i*+4 helical spacings which placed them along the polar face of the amphipathic α -helix of MelP5 (**Fig. S1A**). We screened this library for the most potent macromolecular poration activity and identified the “macrolittins”,¹¹ a novel family of peptides that induce nanoscale pores in lipid bilayers at neutral pH at a strikingly low peptide to lipid ratio (P:L) of \sim 1:1000, **Table 1**. We know of no other peptide with the activity of the macrolittins. In this work, we study three macrolittins, M70, M159 and M204 which have very similar activities, focusing only on M159 in some experiments (**Fig 1A**).

The lipid vesicles used in the evolution of the macrolittins were made from the lipid 1-palmitoyl-2-oleoyl-sn-glycero-3-phosphocholine (POPC). This fluid phase lipid recapitulates many of the physical-chemical properties of mammalian cell plasma membranes, and thus has been widely used for decades as a model system despite the fact that POPC bilayers lack the compositional complexity of biomembranes.¹² Here we test the hypothesis that two generations of synthetic molecular evolution using POPC vesicles have given the macrolittins some selectivity for POPC bilayers over mammalian cell membranes. We find that the macrolittins have no cytolytic activity against human cell lines even at high peptide concentration, despite their very high potency against POPC lipid vesicles at very low concentration. We show that membrane fluidity and thickness, but not headgroup charge, represent the physical-chemical basis for this unprecedented membrane selectivity. Further, we demonstrate translational potential, *in vitro*, by showing that the macrolittin M159 readily triggers the release of macromolecules and small molecule drugs from POPC liposomes in the presence of cells, without affecting the cells directly (**Scheme 1**). We expect that the exquisite membrane selectivity of the macrolittins for POPC liposomes over mammalian cell plasma membranes could be utilized in the triggered release of liposome-encapsulated cargoes in future translational studies.

Experimental Methods

Materials and reagents

Peptides of >95% purity were synthesized by BioSynthesis, Inc. 1-palmitoyl-2-oleoyl-sn-glycero-3-phosphocholine (POPC), 1-palmitoyl-2-oleoyl-sn-glycero-3-phospho-(1'-rac-glycerol) (POPG), 1,2-dioleoyl-sn-glycero-3-phosphoethanolamine-N-[methoxy(polyethyleneglycol)-2000] (PEG2k-PE), 1,2-dimyristoleoyl-sn-glycero-3-phosphocholine (diC14:1PC), 1,2-dieicosenoyl-sn-glycero-3-phosphocholine (C20:1PC), phosphoethanolamine-N-(7-nitro-2-1,3-benzoxadiazol-4-yl) (NBD-PE), 1,2-dioleoyl-sn-glycero-3-phosphoethanolamine-N-(lissamine rhodamine B sulfonyl) (Rhodamine-PE) and Cholesterol were purchased from Avanti Polar Lipids. Labeled low density lipoprotein (BODIPY™ FL LDL), Cholera Toxin Subunit B (Recombinant) with Alexa Fluor™ 488 Conjugate (Labeled CTX), 10 kDa dextran with Alexa Fluor™ 488 Conjugate, 8-Aminonaphthalene-1,2,3-trisulfonic acid (ANTS) and p-xylylenebis (pyridinium bromide) (DPX) were purchased from Thermo Fisher Scientific. Doxorubicin HCl was purchased from Cayman Chemical Company. Chloroform, ammonium thiocyanate, and other salts and buffer materials were purchased from Fisher Scientific or Sigma-Aldrich. TAMRA-biotin-dextran (TBD) was synthesized as described elsewhere.¹³

Peptides

All peptides were synthesized by Biosynthesis Inc and were validated by mass spectrometry and HPLC. Stock solutions of 1.2 mM peptides were prepared with 0.025% acetic acid. Concentrations were determined by measuring the absorbance of the single tryptophan on each peptide. The average of three absorbance measurements at 280 nm on a NanoDrop 2000c (Thermo Fisher Scientific) was used to calculate the concentration. Peptide powders were stored frozen until use and peptide solutions were stored at 4°C.

Liposome Preparation

Large unilamellar vesicles of 100 nm diameter were prepared with different compositions of synthetic lipids. For vesicles without entrapped contents (empty vesicles), lipids in chloroform were dried under vacuum overnight, resuspended in pH 7 buffer (10 mM sodium phosphate, 100 mM KCl, pH=7) to 30-50 mM concentration, and extruded at least 10 times through 100 nm polycarbonate membranes¹⁴. Empty vesicles were used for light scattering, lipid exchange, vesicle fusion, confocal microscope, electric microscopy and cell treatments. Lipid concentration was measured by Stewart Assay.¹⁵

For TBD-entrapping vesicles, dry lipid films were resuspended in buffer containing 1 mg of TBD per 50 μmol of lipid and the solutions were subject to 10 freeze-thaw cycles using liquid nitrogen. After extrusion, vesicles were incubated on high-capacity streptavidin agarose to remove unencapsulated TBD⁹.

For ANTS/DPX or labeled CTX vesicles, dried lipid films were resuspended in 12.5 mM ANTS and 45 mM DPX or 20 μg/ml labeled CTX. Upon extrusion, unencapsulated ANTS and DPX or in labeled CTX were separated from the vesicles by size exclusion chromatography with Sephadex G-100 resin.

For Doxorubicin-containing liposomes, a remote loading method was used¹⁶. POPC and cholesterol (mol/mol = 7/3) were dried under vacuum overnight. The resulting lipid film was hydrated with 300 mM (NH₄)₂HPO₄ solution by gentle mixing, then the generated vesicles were extruded over 10 times through 100 nm polycarbonate membranes. Liposomes were passed through a Sephadex G-100 resin column equilibrated with an isotonic HEPES buffered saline (HBS) including 140 mM NaCl, 10 mM HEPES ([4-(2-hydroxyethyl)-piperazino]-ethanesulfonic acid, pH 7.4) to replace the extra-liposomal solution. The eluted liposomes were diluted with isotonic HEPES buffer to yield a final lipid concentration of 5 mM. Subsequently, doxorubicin HCl was added to the liposomal dispersion to achieve a drug to lipid ratio of 1/3 (mol/mol). The loading process was carried out at 4 °C for 12 h. The separation of liposomes from free DXR was performed by ultracentrifugation. Ultracentrifugation was performed at 130000 × g for 3 h at 20 °C (Beckman Airfuge, USA), and the supernatant was removed. The liposome pellet was redispersed in HBS at pH 7.4.

Light Scattering Assays

2 mM liposomes with different lipid compositions were incubated with M159 or MelP5 for 3 h and 24 h at peptide-to-lipid ratio (P:L) ranging from 1:10 to 1:10000 in 96-well plates, and as a negative control, no peptide was added to liposomes. Absorbance of liposomes by light scattering was measured at 410 nm using a Biotek Synergy plate reader (BioTek, USA). The measurements were repeated three times.

Fluorescence Resonance Energy Transfer (FRET) Assays

0.4 mM Liposomes labeled with 0.5% NBD-PE and 0.5% rhodamine-PE dyes mixed with 2 mM non-labeled liposomes were incubated with MelP5 or M159 for 3 h and 24 h at P:L ranging from 1:10 to 1:10000 in 96-well plates. NBD fluorescence was monitored on a plate reader (ex/em = 480/520 nm), and lipid exchange percentage was calculated by the ratio of measured NBD fluorescence to NBD fluorescence from maximum exchange controls (2.4 mM POPC liposomes containing 0.08 NBD-PE and 0.08% rhodamine-PE), and as a negative control, no peptide was added to mixed liposomes. The measurements were repeated three times. Fractional lipid exchange was calculated as

$$f_{\text{mixing}} = (F_{\text{sample}} - F_{\text{no peptide}}) / (F_{\text{max}} - F_{\text{sample}}) \quad \text{Eq. (1)}$$

Confocal Microscopy

2 mM dye-labeled liposomes and peptides were incubated for 1 hr and a sample was placed on a microscope slide. The distribution of dye-labeled liposomes or dye-labeled proteins were visualized and analyzed using a confocal scanning Nikon Eclipse Ti2 inverted microscope using a 60X oil-immersion objective. Hoest dye staining cell nucleus was excited using a 360 nm laser. NBD, Alexa Fluor® 488, Bodipy dyes were excited using a 488 nm laser. Rhodamine was excited using a 543 nm laser.

Time-lapse Imaging

2 mM NBD labeled 100% POPC liposomes was imaged by confocal microscope immediately after 60 μ M M159 was added in liposome solution. The resultant video consists of 80 images from 0 minute to 40 minutes after M159 addition in a time-lapse manner. (30 seconds per image)

Cryo-transmission Electron Microscopy

Liposome formulations were diluted with the HBS buffer to reach a total lipid concentration of 2 mM and were incubated with peptides for 24 h. Cryo-TEM imaging was done on an FEI G2 F30 Tecnai TEM operated at 150 kV. To prepare the sample, a mesh copper grid (Electron Microscopy Sciences) was picked up with tweezers and mounted on the plunging station of an FEI Vitrobot. Five microliters of the solution were applied to the grid. The excess liquid was blotted by filter paper attached to arms of the Vitrobot for

2 s to form a thin film. The sample was then vitrified by plunging into liquid ethane. The vitrified sample was finally transferred onto a single-tilt cryo specimen holder for imaging.

Macromolecular Leakage Assays

Leakage of 40 kDa TAMRA-biotin-dextran (TBD) was measured using Forster resonance Energy Transfer (FRET) as described^{9, 11, 17}. Dextran vesicles with entrapped TBD were diluted to 1 mM, and streptavidin-AF488 (the donor fluorophore) was added to a final concentration of 20 nM. In a 96-well plate, peptide and vesicles were mixed with P:L ranging from 1:10 to 1:10000 and then incubated while shaking at room temperature for 1 h before measuring FRET by donor fluorescence quenching with ex/em = 495/519 nm. As a positive control for 100% leakage, 4 μ L of 10% Triton X100 was added to three wells, and as a negative control, no peptide was added to three wells. The measurements were repeated three times. Fractional leakage was calculated as

$$f_{\text{TBD leakage}} = (F_{\text{no peptide}} - F_{\text{sample}}) / (F_{\text{no peptide}} - F_{\text{triton}}) \quad \text{Eq. (2)}$$

ANTS/DPX Leakage Assays

Small-molecule leakage was measured by quenching ANTS with DPX. ANTS/DPX leakage vesicles were diluted to 1 mM. On a 96-well plate, peptide and vesicles were mixed at P:L ranging from 1:10 to 1:10000 and then incubated with shaking at room temperature for 1 h before measuring ANTS fluorescence using a microplate reader with ex/em = 360/519 nm. As a positive control for 100% leakage, 4 μ L of 10% Triton X100 was added to three wells, and as a negative control, no peptide was added to three wells. The measurements were repeated three times. Fractional leakage was calculated as¹¹

$$f_{\text{ANTS/DPX leakage}} = (F_{\text{sample}} - F_{\text{no peptide}}) / (F_{\text{triton}} - F_{\text{no peptide}}) \quad \text{Eq. (3)}$$

Tryptophan Binding

100 μ L 10 μ M MelP5 or M159 were prepared in HBS solutions in cuvettes. Liposomes with different lipid compositions were added with P:L ranging from 1:10 to 1:170. After 10 minutes of incubation at room temperature, tryptophan fluorescence spectra were measured on a spectrophotometer (HORIBA, Canada) and the peak fluorescence intensity was recorded at 333 nm (ex = 280 nm). To correct for lipid scattering¹⁸, we measured fluorescence of free tryptophan at P:L ranging from 1:10 to 1:170. The fitting curve and mole-fraction partition coefficient K_p , was obtained by fitting using the equation¹⁹

$$I([L]) = 1 + (K_p[L]) / ([W] + K_p[L]), \quad \text{Eq. (4)}$$

where K_p is a mole-fraction partition coefficient, I is the fluorescence fold increase compared to no lipid binding, $[L]$ is the lipid concentration and $[W] = 55.3 \text{ M}$ is the molar concentration of water. The measurements were repeated three times. And fraction of bound peptides can be calculated as

$$f_{\text{bound}} = (K_p[L])/([W] + K_p[L]) \quad \text{Eq. (5)}$$

Cell Culture

HeLa cells, HepG2 cells, and Raw 264.7 cells were purchased from ATCC. Cells were cultured at 37 °C with 5% CO₂ in Dulbecco's Modified Eagle's Medium (DMEM) (Gibco) supplemented with 10% fetal bovine serum (FBS) (Gibco), 1% antibiotic-antimycotic (Gibco), and 1% non-essential amino acids (Gibco). Cells were passaged 1:5 at 90% confluency.

Cell Toxicity Assays

Cells at 60%-80% cell confluency were treated with peptide or drug for specific periods of time. Cells in 100 μl media in 96-well plate were treated with 10 μl of 10 \times Alamar Blue reagent and incubated for 3 h at 37 °C. The fluorescence (ex570/em585) was measured and compared to mock treated wells.

Human Serum and Erythrocytes

Fresh human serum (OTC) and human O+ erythrocytes were obtained from Interstate Blood Bank, Inc. RBCs were subjected to four cycles of centrifugation at 1000x g with resuspension in fresh DPBS. Following the final wash step, the supernatant was clear and colorless. RBC concentration was determined using a hemocytometer.

Cells Binding

Suspensions of human red blood cells or RAW 264.7 macrophage cells were prepared at increasing cell densities and mixed with stock 20 μM peptide. The suspensions were rocked gently for 30 minutes at RT prior to centrifugation at 10000xg. The peptide remaining in the supernatants was measured with analytical reverse phase HPLC by comparing native tryptophan fluorescence peak areas with controls of known concentration.²⁰

Dextran Uptake Assay

HeLa cells at around 80% cell confluency were incubated with 10 kDa AF488-labeled dextran and different peptides for 30 min, then cells were not washed and were observed using confocal microscopy. (ex488/em512)

Flow Cytometry

After HepG2 cells were treated with liposomes and/or peptides at around 80% cell confluency, the incubation solution was aspirated and cells were released with 100 μ l 0.025% Trypsin for 3 min at 37 °C; 500 μ l DMEM containing 2% FBS, 20 mM HEPES was used to suspend the cells. Cells were transferred to a filter-topped flow cytometry tube and analyzed on a BD LSR II flow cytometer. Cells displaying normal morphologies were gated and analyzed for labeled CTX fluorescence and rhodamine-labeled lipid fluorescence using the 488 nm and the 543 nm laser, respectively.

Doxorubicin Leakage Assays

40 μ l Doxorubicin-containing liposomes were incubated with peptides at different concentrations for 1 h and were subject to ultracentrifugation at 130000 x g for 10 min at room temperature, then doxorubicin in the supernatants were quantified photometrically at 495 nm. Complete liposome lysis was treated with 5 μ l 4% Triton X-100, and as a negative control, no peptide was added. Fractional leakage was calculated as

$$f_{\text{DOX leakage}} = (F_{\text{sample}} - F_{\text{no peptide}}) / (F_{\text{Triton}} - F_{\text{no peptide}}) \quad \text{Eq. (6)}$$

Statistical Analyses

All data were presented as mean \pm standard error (SE) of at least three independent biological experiments (n=3). Graphs were drawn and statistical analyses were performed using GraphPad or Origin.

Results

Interaction between macrolittins and cells

Melittin and the first generation MelP5, like most peptides that permeabilize PC bilayers, also permeabilize cell membranes.²¹ To determine if two generations of synthetic molecular evolution against POPC vesicles have given the macrolittins any selectivity for POPC, we measured the cytolytic toxicity of three macrolittins against various cell types (**Fig. 1**) including human red blood cells (**Fig. 1B**), HeLa human ovarian epithelial cells (**Fig. S2A**), HepG2 human liver epithelial cells (**Fig. S2B**) and Raw 264.7 murine macrophages (**Fig. S2C**). These four cell types were chosen because they represent a variety of organs, have different cell functions, and have different membrane characteristics. Remarkably, despite the highly potent activity of the macrolittins against POPC liposomes, they have no measurable toxicity against any cells even at high concentration (100 μ M). In contrast, the parent peptide MelP5 causes complete cell lysis at 2-5 μ M concentrations (**Fig. 1C**).

To determine if the lack of macrolittin activity in cells is coupled to a lack of binding, we next measured whole cell binding of peptides by label-free binding experiments.²⁰ Our results, in **Fig. 1D**, indicate that macrolittins bind weakly, or not at all, to human red blood cells and to Raw 264.7 macrophages. In contrast, MelP5 peptides bind strongly to both cell types. MelP5 binding to red blood cells could not be measured directly due to interference from released hemoglobin, but the fact that MelP5 permeabilizes these cells at $< 5 \mu\text{M}$ concentration means that it must bind well. Consistent with the lack of toxicity and lack of binding, we show, using confocal microscopy, that dye-labeled dextran (10 kDa) remains excluded from cells in the presence of concentrated M159 or the inert negative control peptide, Oneg.²² By contrast, incubation of cells with MelP5 enables dextran to enter (**Fig. S2D**). Collectively, these results show that M159 does not partition strongly into human cell membranes and does not permeabilize the plasma membranes of human cells, even at high peptide concentration.

Mechanisms underlying membrane selectivity

Macrolittins have a higher potency for releasing macromolecules from synthetic POPC vesicles than MelP5 (Table 1), and yet have a much lower propensity to permeabilize human cell membranes. This selectivity exists despite the fact that 21 of their 26 residues are identical. To determine the factors contributing to this stringent membrane selectivity, we tested hypotheses related to the differences between pure POPC liposomes and mammalian cell membranes.

First, because M159 has a net charge of about -1 at pH 7 while MelP5 has a charge of +3, we hypothesized that the moderate anionic charge on the cell surface, contributed by glycoconjugates on lipids and proteins, plus any external anionic lipids such as phosphatidylserine,²³ might inhibit macrolittin binding. In comparison, POPC bilayers are zwitterionic with zero net charge. To test the hypothesis, we measured MelP5- and M159-induced leakage of small molecules (ANTS/DPX) and macromolecules (TBD 40 kDa) from liposomes containing 95% POPC and 5% anionic POPG to mimic an anionic charged surface. Inclusion of 5% anionic POPG did not significantly change the potency of leakage for small or for large molecules induced by either M159 or MelP5 (**Fig. 2A&E**). Electrostatic repulsion thus does not explain the lack of cytotoxicity.

Second, we hypothesized that hydrocarbon core thickness and fluidity might affect pore formation and that the 20-40 mol% cholesterol in mammalian cell plasma membranes²⁴ might contribute to the lack of cellular activity of the macrolittins. To test this, we measured leakage from POPC liposomes with 30 mol% cholesterol. Inclusion of cholesterol in liposomes, which alters both thickness and acyl chain fluidity, significantly inhibited leakage of both small and large molecules for M159, providing the first clue to the physical chemistry of its membrane selectivity. Interestingly, small molecule leakage for MelP5 was

decreased only slightly by cholesterol (**Fig. 2C**), and macromolecule leakage was actually increased (**Fig. 2G**), consistent with the very potent activity of Melp5 against cholesterol-containing mammalian cell membranes.

Third, we hypothesized that bilayer thickness might strongly affect macrolittin activity in membranes. To test this effect, we prepared liposomes with 100% PC lipids comprised of either diC14:1(9)PC or diC20:1(11)PC lipids. These di-unsaturated PC lipids, like POPC, are both in the fluid phase at room temperature, and have similar acyl chain fluidity. diC14:1-PC forms a thinner bilayer than POPC, while diC20:1-PC forms a thicker bilayer. Against thinner diC14:1-PC bilayers, the potency M159-induced leakage of TBD decreased by a small amount. **Fig. 2D**. Against thicker diC20:1-PC bilayers, the potency of M159 for macromolecular poration was dramatically reduced, **Fig. 2H**. Melp5 was less sensitive to bilayer thickness. In diC14:1PC its activity is similar to POPC, and in diC20PC bilayers its activity was reduced, but not as much as M159.

Fourth, we hypothesized that the crowded carbohydrate layer on mammalian cell membranes²⁵ could inhibit macrolittin binding and activity. To mimic this effect, we measured liposome permeabilization using POPC liposomes containing 5% lipids with a covalently attached 2,000 Da polyethylene glycerol (PEG2k-PE). At 5 mol%, PEG2k fully covers the surface of a lipid vesicle with a continuous PEG layer in the “mushroom” configuration.²⁶ Inclusion of 5% PEG2k-PE did not change the potency of either small or large molecule leakage induced by either M159 or Melp5 (**Fig. 2B&F**).

Collectively, the extraordinary selectivity of the macrolittins for POPC liposomes over cell membranes, is based on membrane properties that affect the hydrocarbon core of the membrane, including cholesterol content and membrane thickness.

Liposomal aggregation and fusion induced by peptides

To realize our long-term goal of utilizing macrolittins for triggered release *in vivo*, we must control the fate of liposomes that have been permeabilized by macrolittins. Pore-forming peptides often cause fusion and aggregation of lipid vesicles because they disrupt the normally strict segregation of polar and nonpolar moieties in the bilayer.²⁷ To investigate the effects of macrolittins on POPC vesicle architecture, we first measured light scattering by optical absorbance, which will increase if average particle size increases due to aggregation or fusion.²⁸ The results, in **Fig. 3A**, show that M159 induces significant aggregation or fusion of POPC liposomes even at very low P:L, with a maximum light scattering at P:L ~ 0.015. For comparison Melp5 caused little change in light scattering at any concentration. The decrease in light scattering from the peak with increasing P:L probably results from the partial solubilization of the bilayers by macrolittin at these high concentrations.¹¹ To test whether the macrolittin-induced increase in light scattering is due to

membrane fusion, we measured lipid exchange using Förster resonance energy transfer (FRET) between dye-labeled lipids.²⁹ In this assay, NBD-lipid fluorescence is quenched by rhodamine-labeled lipids in dye-labeled vesicles. Labeled vesicles are mixed with an excess of unlabeled vesicles and peptide such that NBD fluorescence will increase if fusion takes place due to dilution of the donor and acceptor lipids into the unlabeled liposomes. The measurements in **Fig. 3B** show that M159 causes significant vesicle fusion while MelP5 causes much less fusion. To further characterize the effects of M159 and MelP5 on vesicle architecture, we observed liposomes using confocal microscopy and cryo electron microscopy. In confocal microscopy, individual dye-labeled liposomes with 0.1 μm diameter cannot be resolved, leading to a diffuse fluorescent background. However, after addition of M159, we observed the formation of very large ($\geq 10 \mu\text{m}$) irregular structures (**Fig. 3C**). The size of the aggregates depended on peptide to lipid ratio when P:L < 0.003 (**Fig. S3**). To characterize the process of liposome aggregate growth, we also monitored aggregation as a function of time. Upon M159 addition, aggregation and fusion began immediately. Lipid aggregates grew as large as 20 μm within 40 minutes (**Supplementary Video**). Addition of MelP5 to POPC vesicles generated only a few visible aggregates. CryoEM results show that addition of M159 to 0.1 μm unilamellar POPC vesicles results in the formation of large multilamellar vesicles, verifying that membrane fusion is driving changes in membrane topology. MelP5 does not cause the formation of multilamellar vesicles (**Fig. 3D**).

If macromolecular poration and bilayer fusion are elements of the same mechanism, then they will probably have the same membrane selectivity. To test this, we performed light scattering and FRET assays using liposomes containing 30% cholesterol. The results (**Fig. 4A**) showed that M159 causes only a small amount of aggregation and fusion in 30% cholesterol bilayers, matching its low macromolecular poration activity in the same bilayers (**Fig. 2G**). MelP5, on the other hand, induced more liposome aggregation and fusion in POPC bilayers containing 30% cholesterol (**Fig. 4B**) compared to POPC, just as it caused more leakage (**Fig. 2G**). To further test the effect of cholesterol on macrolittin fusion activity, we also tested for peptide-induced fusion and aggregation of low-density lipoprotein (LDL) particles, which are bounded by a cholesterol rich lipid monolayer.³⁰ M159 does not cause aggregation of LDL particles, while MelP5 causes dramatic increases in LDL particle size (**Fig. 4C**), consistent with the observed selectivity of these peptides in experiments with lipid vesicles.

Blocking peptide-induced lipid-lipid interaction.

Fusion and aggregation of POPC vesicles would be an undesirable effect in triggered release *in vivo* because peptide-destabilized vesicles can interact with cells and deposit lipids in tissues. Such vesicles will also have altered shape and increased size and thus altered and unpredictable circulation times and clearance routes.³¹ Therefore, we next tested whether fusion and aggregation can be inhibited, without changing

nanoscale pore formation and macromolecular cargo release. In these experiments, we also test the hypothesis that macromolecule release is due only to pore formation and is not the incidental result of fusion and aggregation. Earlier, in **Fig. 2**, we showed that the addition of 5% anionic lipids or the addition of 5% PEG2k-PE lipids to POPC do not inhibit macromolecular poration. At the same time, these lipids are expected to decrease fusion and aggregation of vesicles, due to the added electrostatic and steric repulsion between membrane surfaces, respectively.²⁷ Thus, we tested the effect of addition of either 5 mol% POPG or 5% PEG2k-PE on aggregation and fusion and showed that these lipids essentially eliminate M159-dependent changes in particle size (**Fig. S4A**), and significantly reduce fusion between vesicles (**Fig. S4B**). Yet, they do not change binding of macrolittins (**Fig. S5**) and they do not change nanoscale poration (**Fig. 2**). Thus, fusion and aggregation are easily mitigated without any loss of membrane selectivity or macromolecular poration of liposomes. We also tested the effects of macrolittins on liposome-cell interactions. We incubated cultured human HeLa cells with dye-labeled liposomes made from 100% POPC, POPC + 5% POPG, or POPC + 5% PEG2k-PE. We found that liposomes containing 5% PEG2k-PE interact very little with cells compared to POPC and POPC+POPG liposomes, in the presence of M159 (**Fig. S4C**). Based on these experiments, we conclude that inclusion of 5% PEG2k-PE lipids in POPC vesicles will dramatically reduce fusion or aggregation in the presence of cells. Thus, in the cell culture experiments that follow below, we used POPC + 5 mol% PEG2k-PE to prevent liposome cell interactions.

M159 releases cargoes from liposomes in cell culture

Based on the data above, we hypothesized that macrolittins could be used to trigger macromolecular cargo release from POPC-PEG liposomes in the presence of cells without directly affecting the cells and without causing vesicle aggregation or fusion with cells. To test this idea, we used fluorescein-labeled cholera toxin subunit B (Fl-CTXB) as a macromolecular cargo. Fl-CTXB, which has a molecular weight of 11.6 kDa, binds strongly to GM1 sphingolipids on cell membranes and is actively endocytosed.³² We chose to use HepG2 liver epithelial cells in this experiment because cholera toxin subunits undergo more efficient and more rapid endocytosis in liver and hepatoma cells compared to other cell types.³³ We measured release from liposomes and subsequent cellular uptake using flow cytometry. We also determined the subcellular location of the released cargo by confocal microscopy. Fl-CTXB, at 0.7 $\mu\text{g/ml}$, was encapsulated in POPC vesicles containing 5% PEG2k-PE. We added vesicles with entrapped CTXB to HepG2 cells, followed by addition of M159. For a positive control we used direct addition of the same amount of non-encapsulated CTXB plus vesicles. For negative controls, we used vesicles and cells plus either no peptide addition, or the addition of the inert peptide Oneg. The imaging and flow cytometry results show that M159 readily released all Fl-CTXB from vesicles, while the negative controls did not, and that the released protein was intact and was quickly uptaken into cells by endocytosis (**Fig. 5A&B**).

In the same experiments, we measured cell uptake of liposomes or fusion with cell membranes by using vesicles doped with rhodamine lipids. For a positive control, we used R18, non-toxic rhodamine-C18 fatty acid dye, which inserts into cell membrane spontaneously. The amount of R18 added was equal to the rhodamine lipids present in the system. By comparison, less than 1% of the R18 lipid in liposomes became associated with cells, during 100% FI-CTXB release and uptake, verifying that fusion and aggregation with cells do not take place during this triggered release experiment (**Fig. 5C**).

Doxorubicin (DXR) is a small molecule chemotherapy drug widely used against breast, uterine, ovarian, lung and cervical cancer.³⁴ We also showed controlled release of DXR which is encapsulated into cholesterol-containing liposomes using a remote loading method by a transmembrane phosphate gradient.¹⁶ We chose HeLa cell lines from cervical cancer to test DXR releasing efficiency given that these cells are highly sensitive to DXR. First, we confirmed that DXR encapsulation in these liposomes is stable for at least 24 hours (**Fig. S6A**). Then we measured peptide-induced leakage at 37°C and showed that M159 can induce release of DXR from these PC/cholesterol vesicles (**Fig. 6A**), despite its reduced activity against cholesterol containing bilayers. Subsequently, we identified that the minimal exposure time for 200 µM free DXR to enter HeLa cells and cause measurable HeLa cell toxicity is 12 minutes (**Fig. S6B**). In these experiments, we added 200 µM vesicle-encapsulated DXR to HeLa cells and then induced drug release by adding M159 to the system for only 15 minutes before washing off vesicles and peptides. Positive control was 200 µM free DXR. Negative control was vesicle-encapsulated DXR plus the inert peptide Oneg. Confocal microscopy showed that DXR was released from liposomes by M159 and was bound to DNA in the cell nucleus after 15 min incubation (**Fig. 6B**). To quantify the cell toxicity induced by DXR, cells were treated with free DXR or encapsulated DXR plus peptides and then cytotoxicity was measured. Treatment of HeLa cells for 15 minutes with 200 µM encapsulated DXR plus M159 had the same toxic effect as 200 µM free DXR (**Fig. 6C&S6C**), demonstrating that M159 readily made 100% of the vesicle entrapped cargo available for bioactivity in the presence of cells. Collectively, these experiments constitute a demonstration that the selectivity of the macrolittins is sufficient to trigger the release of small molecules and macromolecules from liposomes in the presence of cells, such that the cargo is immediately made available to interact with cells.

Discussion

We have used synthetic lipid vesicles made from the lipid POPC for the evolution of multiple classes of membrane active peptides, including the evolution of MelP5 from melittin and evolution of the macrolittins from MelP5.^{6, 11} POPC is an appropriate and widely used physical-chemical mimic of eukaryotic plasma

membranes. First, PC is the most abundant lipid headgroup in cell plasma membranes. Second, saturated 16 carbon fatty acids and monounsaturated 18 carbon fatty acids on the glycerol sn-1 and sn-2 carbons, respectively, are among the most common fatty acids in mammalian phospholipids.³⁵ Like most cell membrane phospholipids, POPC exists as a lamellar liquid crystalline fluid phase bilayer at physiologically relevant temperatures. POPC supports folding and function of mammalian membrane proteins because it mimics the generic physicochemical properties of mammalian membranes. However, maximal function of reconstituted membrane proteins sometimes requires specific lipid compositions.³⁶ Although the average properties of cell plasma membranes are mimicked by POPC, cell membranes are much more complex, composed of many diacyl lipid species, neutral, zwitterionic and anionic, as well as cholesterol.³⁷ Cell membranes also contain many membrane proteins, and are separated into a mosaic of domains with different lipid compositions.^{38, 39} Finally, unlike POPC, cell plasma membranes are somewhat anionic on the external surface, mostly due to a crowded surface layer of anionic glycoconjugates attached to both lipids and proteins.

The differences in membrane selectivity between M159 and its predecessors can be quantified by comparing potencies that are relevant to our translational goals; triggered release of macromolecules from POPC vesicles versus toxic cytolysis of cell membranes. For the release of a 40 kDa dextran from POPC, M159 is about 30-fold more potent than MelP5 and at least 100-fold more potent than melittin (**Table 1 & Fig. 2**). On the other hand, M159 is at least 250-fold less potent than MelP5 or melittin against human cell membranes (**Fig. 1**). After just two generations of synthetic molecular evolution, M159 is at least 7,500-fold more selective than MelP5, and 25,000-fold more selective than melittin, for POPC vesicles over human cell plasma membranes.

There is a critical difference between the macrolittins and most other membrane permeabilizing peptides that provides an important clue about the mechanism of their membrane selectivity. The macrolittins release both small molecules and macromolecules from POPC bilayers with similar high potencies (**Fig. 2**). This is very unusual, as most membrane permeabilizing peptides, including melittin and MelP5, release small molecules (< 500 Da) at much lower P:L than they release macromolecules.⁹ The majority of membrane permeabilizing peptides do not form explicit nanoscale pores in membranes at all, but act through what we have called “interfacial activity”⁴⁰ to form a continuum of transient, dynamic and heterogeneous permeabilization pathways through the membrane. Typically, the maximum size of released molecules increases with P:L, giving rise to different potencies for small molecule and macromolecule release. We have shown by atomic force microscopy that macrolittins form a range of nm-sized pores in POPC bilayers, but do not appreciably form sub-nm pores or local bilayer perturbations that are selective for small molecules.¹¹ Taken together, these observations show that macrolittins self-assemble only into nm-sized

pore structures, with a size around ~ 1 nm. They do not form intermediate structures that release small molecules only.

By evolving peptides over two generations in POPC vesicles for macromolecule release at low concentration, we have likely created a unique nanoscale pore structure that is especially well-suited to form large pores in POPC bilayers. Once inserted across the membrane, the peptides likely form a boundary between the large aqueous pore and the bilayer lipids by orienting the three acidic residues and two basic residues on the hydrophilic surface of the α -helix towards the pore interior, while the hydrophobic surface is oriented toward the membrane lipids. In this model, the free energy of the peptide-lipid and peptide-peptide interfaces will be critically important for pore stability. The sensitivity of pore formation to the hydrocarbon core properties (i.e. cholesterol content and bilayer thickness), and thus the membrane selectivity of the macrolittins, are probably the result of this unique large pore architecture as its stability will depend on hydrophobic length matching between bilayer and peptide.⁴¹

Based on these ideas, we can speculate that MelP5 has a hybrid mechanism, sharing elements of the selective “daughter” macrolittins as well as with the non-selective “parent” melittin. Unlike the macrolittins, MelP5 releases small molecules at much lower concentrations than it releases macromolecules, a property it shares with its parent peptide melittin (**Fig. 1**).⁴² Yet, at higher concentrations, MelP5 can self-assemble into nm-sized membrane spanning pores, like the macrolittins.⁴³ Thus, we speculate that MelP5 permeabilizes POPC with a continuum of membrane-permeabilizing activities, including non-specific membrane permeabilization to small molecules at the lowest concentrations and self-assembly into macromolecule-sized pores at higher concentrations. Because it forms a continuum of structures, MelP5 is much less membrane selective. Interestingly, compared to POPC, MelP5 has increased macromolecule poration activity against cholesterol-containing synthetic bilayers, as well as against cell membranes, and LDL particles. The structural basis for this effect of cholesterol is not fully understood.

Liposomal encapsulation is an effective drug delivery approach in some clinical applications. Several applications are approved for clinical use and many others are in clinical trials.⁴⁴ For example, one recently approved SARS-CoV2 mRNA vaccine is delivered as liposome-encapsulated mRNA for stability.⁴⁵ Some small molecule drugs (e.g doxorubicin and amphotericin B) can diffuse out of liposomes spontaneously for controlled slow release. But many other potential cargoes, including radionuclides and macromolecular cargoes, must be released orthogonally by active means because they do not spontaneously escape. This has prompted the development of vesicles that can be destabilized by various exogenous triggers. However, there are some shortcomings with current triggered release methods. Firstly, the synthesis of specialized lipids and preparation of liposomes subject to such triggered release is often complex. For example, many thermosensitive liposomes include metallic nanoparticles within the artificial membrane.⁴⁶ Secondly,

external stimuli must be localized to the affected tissue, and thus the locations in the body of the affected tissues must be known in advance and must be accessible to external stimuli. Lastly, some liposomes with specific structures or compositions can only encapsulate specific cargoes but not all macromolecular cargoes.⁴⁷ In contrast, we have shown here that the synthetically evolved macrolittins readily trigger release of macromolecules from ordinary POPC-PEG liposomes without interacting with cells and without causing interactions between pegylated-liposomes and cells.

Conclusions

In this work, we have demonstrated a potential triggered release strategy based on the use of the macrolittin family of peptides to trigger cargo release from simple PC liposomes. The macrolittins have unprecedented membrane selectivity and potency to form nanoscale pores in such liposomes, and can release various cargoes in the presence of cells without directly affecting the cells. Further, we showed that addition of PEG lipids eliminated macrolittin-induced fusion and aggregation of vesicles without affecting cargo release. This enables the use of PEG liposomes, which are widely used to extend *in vivo* stability.^{1, 48} Although technical challenges and impediments to clinical application remain, future technologies that may be possible include optimization of enhanced permeability and retention of vesicles and affinity targeting of vesicles to sites of interest. It may also be possible to affinity target macrolittins to specific sites for localized triggered release. For the macrolittins, completely protease resistant D-amino acid variants can be used *in vivo*⁴⁹ because D-macrolittins have the same activity as L-macrolittins. This will significantly extend their bioavailability. Despite the fact that systematic toxicity, tissue accumulation and excretion pathways of macrolittins have yet to be studied carefully, this work supports the idea that the peptide-triggered release of macromolecular cargoes from POPC-PEG liposomes by the macrolittins is a delivery strategy that may be applicable in future translational applications.

Acknowledgements

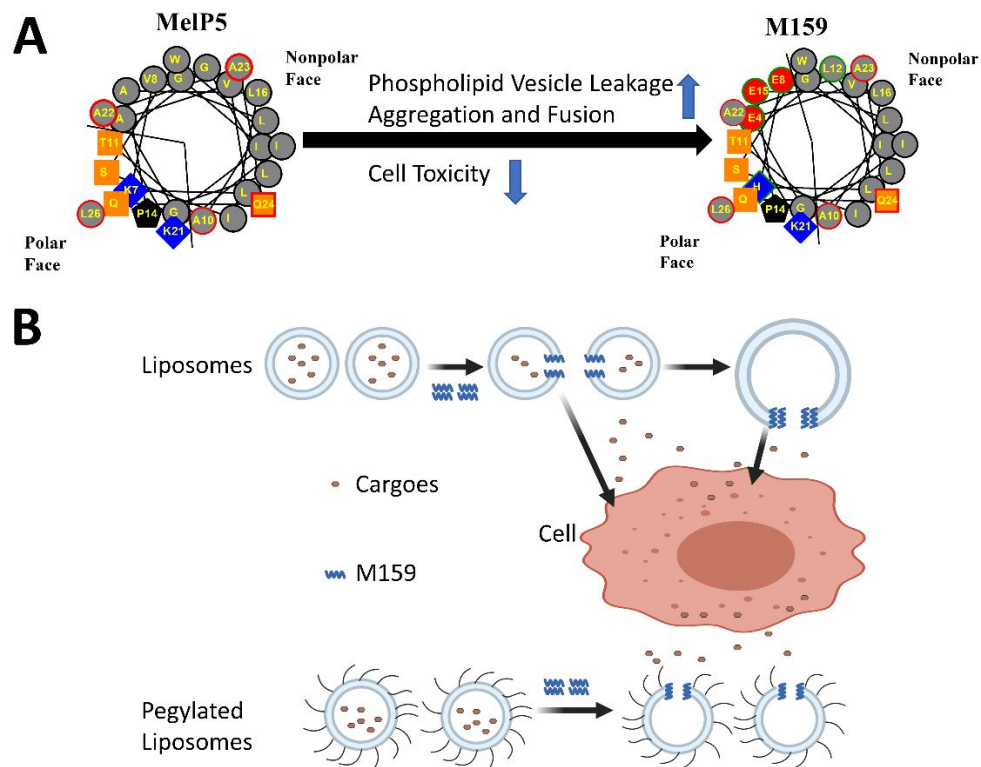
This work was funded by NIH R01 GM111824 and NSF DMR 1710053 (WCW), and NSF DMR 1709892 (KH).

Author contributions

L.S. conducted all of the experiments and analyzed the data. W.C.W, K.H. and L.S designed the study, interpreted the data, and provided resources and funding for the study. All authors contributed to manuscript writing.

Conflicts of interest

There are no conflicts to declare.



Scheme 1. Schematic illustration of M159-induced cargo release from vesicles. **A.** Daughter M159 has a higher membrane selectivity than parent MelP5. **B.** In addition to causing PC vesicle leakage, M159 induces vesicle-vesicle fusion and vesicle-plasma membrane association, but these are inhibited by PEG on vesicles.

Table 1: Comparison of peptide potency trigger 50% probes release from POPC vesicles. POPC vesicles containing small molecules (0.4 kDa) or macromolecules (40 kDa) were permeabilized with three generations of peptides, and peptide to lipid ratios to induce 50% probe release were calculated.^{9, 11}

Peptide	0.4 kDa Probe	40 kDa Probe	Equilibrium TM Pores
Mellitin	1:200	>1:20	No
MelP5	1:2000	1:65	Yes
M159	1:2000	1:2000	Yes

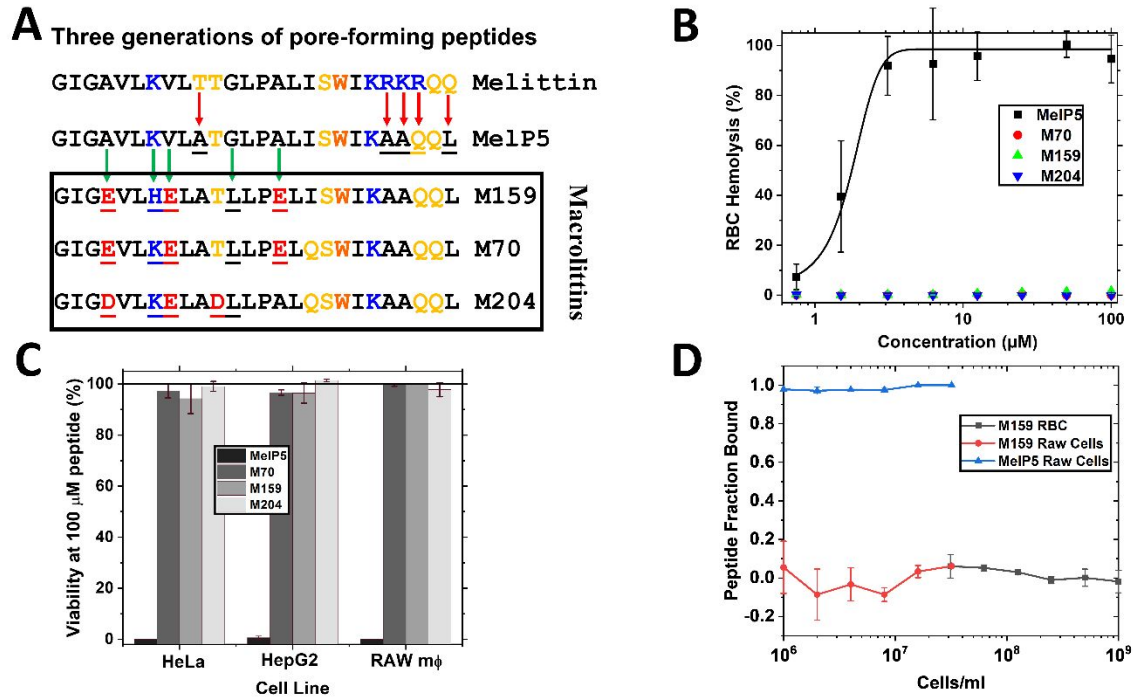


Figure 1. Macrolittins and cell toxicity. **(A)** Sequences of three generations of peptides. The 5 residues that are different between melittin and MelP5 are shown by red arrows and the five residues that are different between MelP5 and the macrolittin M159 are shown by green arrows. Residue colors are black for hydrophobic, red for acidic, blue for basic, and orange for polar & uncharged amino acids. **(B)** Hemolysis of human red blood cells. Serially diluted MelP5 and three macrolittins were incubated with human RBCs for 1 h. Release of hemoglobin was measured using optical absorbance of the cell supernatant at the heme absorbance wavelength of 410 nm, and % lysis against human erythrocytes was shown. **(C)** Three mammalian cell lines (HeLa, HepG2 and Raw macrophage cells) were incubated with different peptides shown at around 80% confluency for 3 h. Summary toxicity data showing % toxicity against three cell lines. **(D).** Measurement of peptide binding to Raw macrophage cells and human red blood cells. 20 μM MelP5 or M159 were incubated with increasing concentrations of cells for 30 min, followed by centrifugation of the cells. Peptide remaining in the supernatant was analyzed by HPLC, and the peptide peak area was compared to that of an identically treated sample without cells to obtain fraction bound.

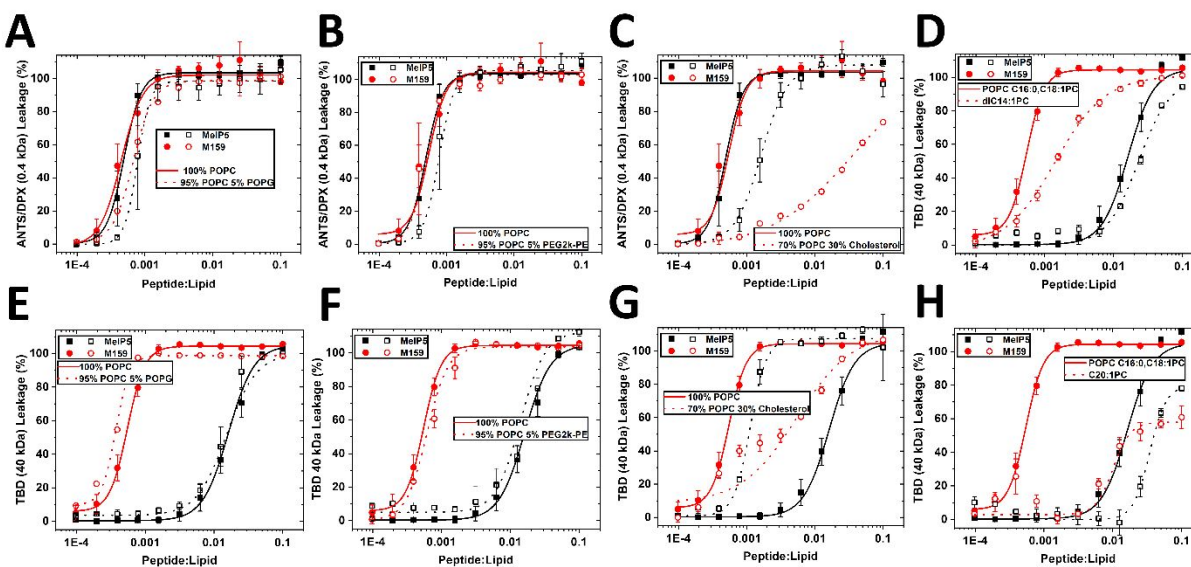


Figure 2. Mechanisms underlying membrane selectivity of macrolittins. **A-C.** ANTS/DPX small molecule leakage results. MelP5 or M159 were incubated with liposomes composed of 100% POPC or 95% POPC and 5% POPG (A); 95% POPC and 5% PEG2k-PE (B); 70% POPC and 30% Cholesterol (C). Vesicles contained encapsulated ANTS (fluorophore) and DPX (quencher). Results are measured after 1 hour. **D-H.** Macromolecular TAMRA-Biotin-Dextran 40 kDa (TBD) leakage assay. MelP5 or M159 were incubated with different compositions of liposomes, 100% POPC or 100% diC14:1PC (D); 95% POPC and 5% POPG (E); 95% POPC and 5% PEG2k-PE (F); 70% POPC and 30% Cholesterol (G); 100% diC20:1-PC (H). Vesicles contain entrapped TBD and AlexaFluor488-streptavidin is added to the external solution. Results are shown after 1 hour incubation. In all experiments, Triton X100 was added to obtain the 100% leakage value as a positive control.

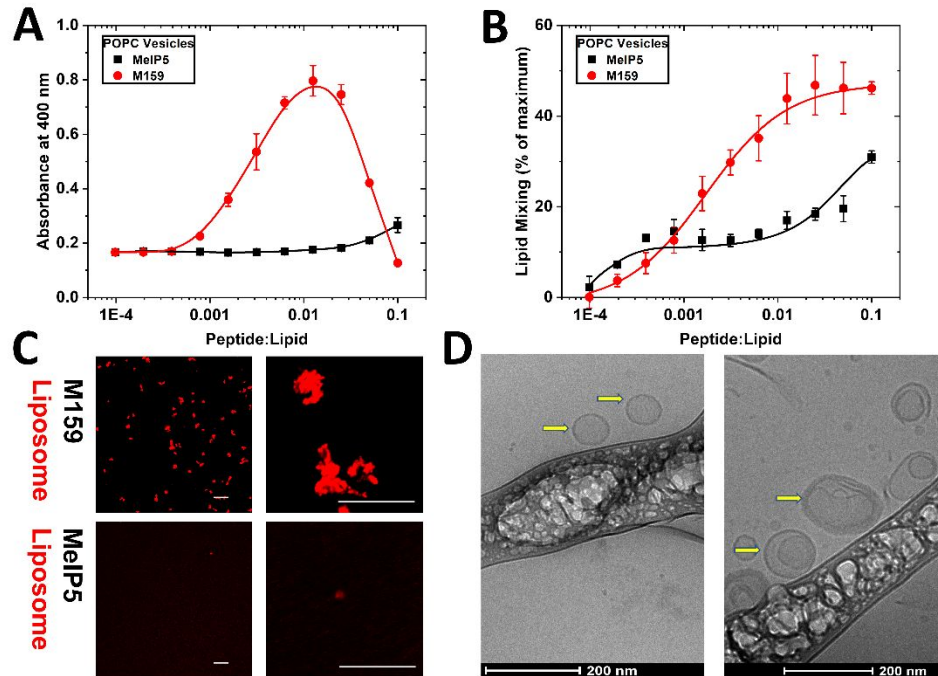


Figure 3. M159-induced aggregation and fusion between pure POPC liposomes. **(A)** Light scattering of POPC liposomes incubated with peptides. 2 mM POPC liposomes were incubated with MelP5 or M159 for 3 h at different peptide-to-lipid ratios. Optical absorbance was measured at 410 nm on a plate reader. **(B)** FRET between dual labeled POPC liposomes and non-labeled POPC liposomes. 0.4 mM POPC liposomes containing 0.5% NBD-PE and 0.5% rhodamine-PE dyes mixed with 2 mM pure POPC liposomes were incubated with MelP5 or M159 for 3 h at different peptide-to-lipid ratios. NBD fluorescence was monitored on a plate reader and lipid exchange percentage was calculated by the ratio of measured NBD fluorescence to NBD fluorescence from positive controls **(C)** Confocal microscopy images of POPC liposomes. 2 mM rhodamine-labeled POPC liposomes were incubated with 60 μ M MelP5 or M159 and were observed using confocal microscopy. (Scale bars = 20 μ m) **(D)** Cryo-TEM images of POPC liposomes. 2 mM POPC liposomes were incubated with 60 μ M MelP5 (left) or M159 (right) and were visualized by Cryo-TEM. Liposomes are indicated by yellow arrows.

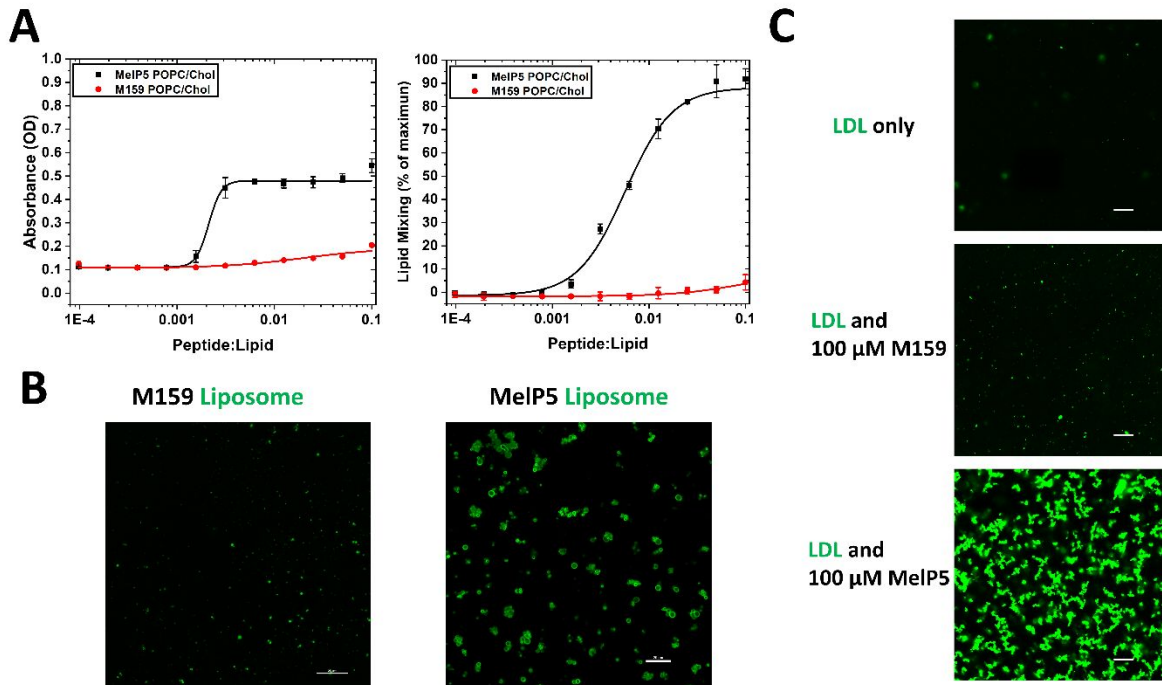


Figure 4. Melp5-induced aggregation of liposomes containing cholesterol. (A) Light scattering of liposomes made of 50% POPC and 50% cholesterol is recorded in response to Melp5 (left). Lipid exchange in liposomes made of 50% POPC and 50% cholesterol is induced by Melp5 (right). (B) 2 mM NBD-labeled liposomes made of 70% POPC and 30% cholesterol were incubated with 20 μ M Melp5 or M159 and were observed in a confocal microscope (Left: M159 treatment; right: Melp5 treatment). (C) 10 μ g/ml Bodipy-labeled LDL (ex/em = 488/512 nm) was incubated with 100 μ M M159 or Melp5 for 3 h at 37 degrees. The LDL particles were observed in a confocal microscope (top: LDL alone; middle: LDL and M159; bottom: LDL and Melp5). Scale bar = 20 μ m.

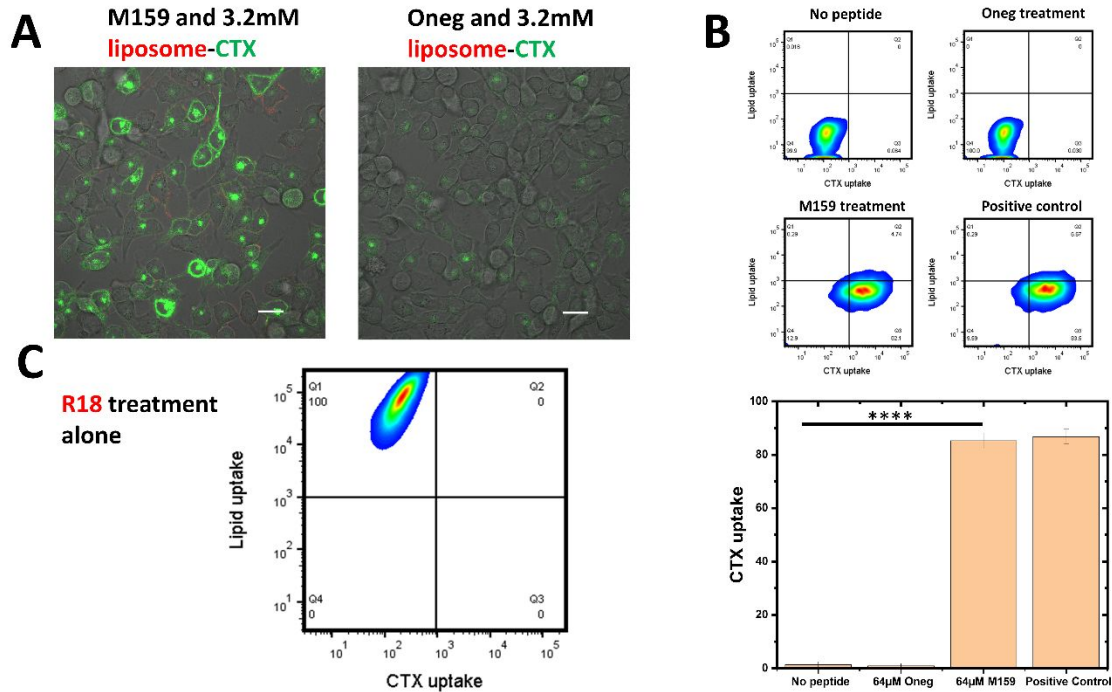


Figure 5. The effect of M159 on liposomes containing cholera toxin subunit B (CTXB). **(A)** 3.2 mM 0.1% rhodamine-labeled liposomes (95% POPC, 5% PEG2k-PE) containing 0.7 mg/L FITC-CTXB were incubated with cells for 5 min and then 64 μ M M159 or Oneg were added to HepG2 cells at around 80% cell confluency. After 25 min, cells were washed and observed in a confocal microscope (ex/em = 488/512 nm) (left: M159 treatment; right: Oneg treatment). Scale bar = 20 μ m. **(B)** Quantification of CTXB and lipid uptake in **A** by cells, using flow cytometry (from left to right: M159 and liposome-CTXB; M159, 0.7mg/L free CTXB and empty liposomes; liposome-CTXB only; Oneg and liposome-CTXB; 3.2 μ M rhodamine R18 lipid). **(C)** Quantification of CTXB uptake. Each measurement was repeated three times. (****, $p < 0.0001$).

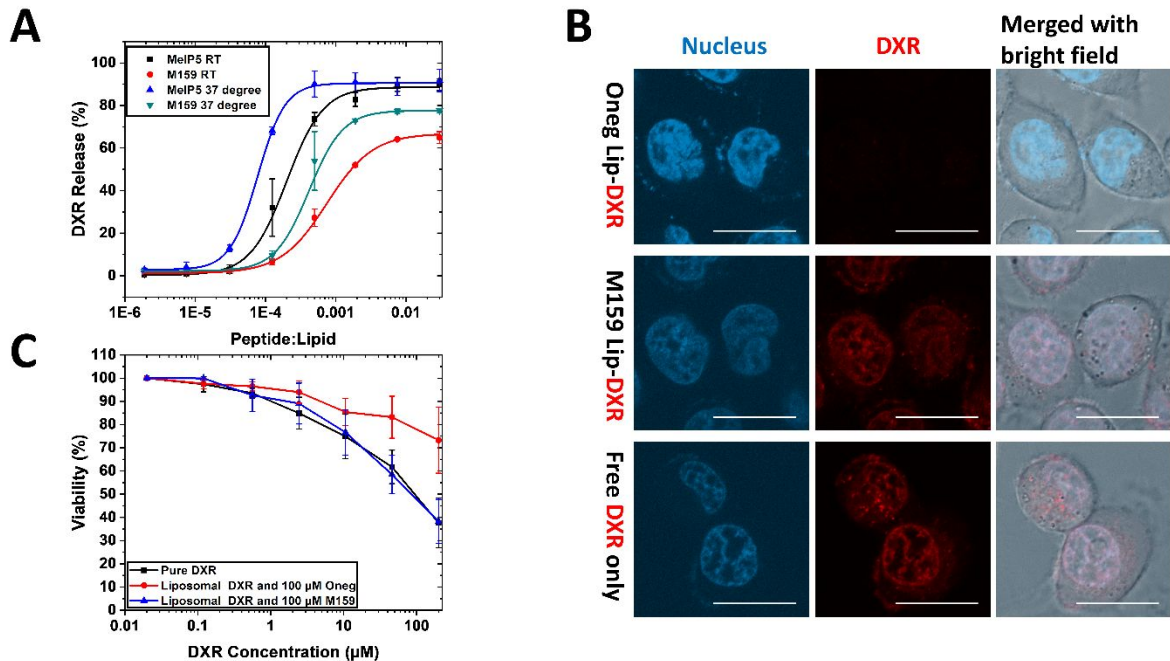


Figure 6. Effect of M159 and liposomes containing Doxorubicin (DXR) on HeLa cells. **(A)** 6 mM liposomes (70% POPC, 30% Chol) containing 600 μM DXR were incubated with increasing concentrations of MelP5 or M159 for 1 h at room temperature or 37 degrees. After ultra-centrifugation, supernatants were measured photometrically at 495 nm by as released DXR. DXR from the lysis of liposomes with Triton X-100 was set as 100% DXR release. **(B)** 2 mM liposomes containing 200 μM DXR were incubated with cells for 5 min, then 100 μM M159 or Oneg was added to cells at around 80% cell confluency. After 15 min, cells were washed and observed in a confocal microscope. Scale bar = 20 μm . **(C)** Quantification of DXR-induced cell toxicity. Increasing concentrations of liposomes containing DXR or increasing concentrations of free DXR were incubated with cells for 5 min, then 100 μM M159 or Oneg was added to the cells. After 15 min, cells were washed and incubated with complete media. After 24 hours, cells were subjected to a cell viability assay.

References

1. R. van der Meel, M. H. Fens, P. Vader, W. W. van Solinge, O. Eniola-Adefeso and R. M. Schiffelers, *J Control Release*, 2014, **195**, 72-85.
2. J. W. Park, *Breast Cancer Res*, 2002, **4**, 95-99.
3. W. C. Zamboni, A. C. Gervais, M. J. Egorin, J. H. Schellens, E. G. Zuhowski, D. Pluim, E. Joseph, D. R. Hamburger, P. K. Working, G. Colbern, M. E. Tonda, D. M. Potter and J. L. Eiseman, *Cancer Chemother Pharmacol*, 2004, **53**, 329-336.
4. Y. Lee and D. H. Thompson, *Wiley Interdiscip Rev Nanomed Nanobiotechnol*, 2017, **9**.
5. S. Guha, J. Ghimire, E. Wu and W. C. Wimley, *Chem Rev*, 2019, **119**, 6040-6085.
6. A. J. Krauson, J. He and W. C. Wimley, *J Am Chem Soc*, 2012, **134**, 12732-12741.
7. R. Smith, F. Separovic, T. J. Milne, A. Whittaker, F. M. Bennett, B. A. Cornell and A. Makriyannis, *J Mol Biol*, 1994, **241**, 456-466.
8. E. Jamasbi, S. Batinovic, R. A. Sharples, M. A. Sani, R. M. Robins-Browne, J. D. Wade, F. Separovic and M. A. Hossain, *Amino Acids*, 2014, **46**, 2759-2766.
9. G. Wiedman, T. Fuselier, J. He, P. C. Searson, K. Hristova and W. C. Wimley, *J Am Chem Soc*, 2014, **136**, 4724-4731.
10. A. J. Krauson, O. M. Hall, T. Fuselier, C. G. Starr, W. B. Kauffman and W. C. Wimley, *J Am Chem Soc*, 2015, **137**, 16144-16152.
11. S. Li, S. Y. Kim, A. E. Pittman, G. M. King, W. C. Wimley and K. Hristova, *J Am Chem Soc*, 2018, **140**, 6441-6447.
12. Q. Lin and E. London, *PLoS One*, 2014, **9**, e87903.
13. W. C. Wimley, *Methods Mol Biol*, 2015, **1324**, 89-106.
14. L. D. Mayer, M. J. Hope and P. R. Cullis, *Biochim. Biophys. Acta*, 1986, **858**, 161-168.
15. J. C. Stewart, *Anal Biochem*, 1980, **104**, 10-14.
16. A. Fritze, F. Hens, A. Kimpfler, R. Schubert and R. Peschka-Süss, *Biochim Biophys Acta*, 2006, **1758**, 1633-1640.
17. G. Wiedman, S. Y. Kim, E. Zapata-Mercado, W. C. Wimley and K. Hristova, *J Am Chem Soc*, 2017, **139**, 937-945.
18. A. S. Ladokhin, S. Jayasinghe and S. H. White, *Anal. Biochem*, 2000, **285**, 235-245.
19. S. H. White, W. C. Wimley, A. S. Ladokhin and K. Hristova, *Methods Enzymol*, 1998, **295**, 62-87.
20. C. G. Starr, J. He and W. C. Wimley, *ACS Chem Biol*, 2016, **11**, 3391-3399.
21. H. Raghuraman and A. Chattopadhyay, *Biosci Rep*, 2007, **27**, 189-223.
22. J. Cruz, M. Mihailescu, G. Wiedman, K. Herman, P. C. Searson, W. C. Wimley and K. Hristova, *Biophys J*, 2013, **104**, 2419-2428.
23. T. Yeung, G. E. Gilbert, J. Shi, J. Silvius, A. Kapus and S. Grinstein, *Science*, 2008, **319**, 210-213.
24. S. Raffy and J. Teissié, *Biophys J*, 1999, **76**, 2072-2080.
25. J. Chen, J. Gao, M. Cai, H. Xu, J. Jiang, Z. Tian and H. Wang, *Nanoscale*, 2016, **8**, 13611-13619.
26. O. Garbuzenko, Y. Barenholz and A. Prie, *Chem Phys Lipids*, 2005, **135**, 117-129.
27. G. Cevc and H. Richardsen, *Adv Drug Deliv Rev*, 1999, **38**, 207-232.
28. C. S. Chong and K. Colbow, *Biochim Biophys Acta*, 1976, **436**, 260-282.
29. D. K. Struck, D. Hoekstra and R. E. Pagano, *Biochemistry*, 1981, **20**, 4093-4099.
30. T. Hevonjoja, M. O. Pentikäinen, M. T. Hyvönen, P. T. Kovanen and M. Ala-Korpela, *Biochim Biophys Acta*, 2000, **1488**, 189-210.
31. C. Huang, D. Quinn, Y. Sadovsky, S. Suresh and K. J. Hsia, *Proc Natl Acad Sci U S A*, 2017, **114**, 2910-2915.
32. I. Basu and C. Mukhopadhyay, *Langmuir*, 2014, **30**, 15244-15252.
33. C. Merlen, D. Fayol-Messaoudi, S. Fabrega, T. El Hage, A. Servin and F. Authier, *Febs j*, 2005, **272**, 4385-4397.
34. Y. Xue, W. Niu, M. Wang, M. Chen, Y. Guo and B. Lei, *ACS Nano*, 2020, **14**, 442-453.

35. J. E. Vance, *Traffic*, 2015, **16**, 1-18.
36. M. Opekarová and W. Tanner, *Biochim Biophys Acta*, 2003, **1610**, 11-22.
37. T. Harayama and H. Riezman, *Nat Rev Mol Cell Biol*, 2018, **19**, 281-296.
38. V. Kiessling, C. Wan and L. K. Tamm, *Biochim Biophys Acta*, 2009, **1788**, 64-71.
39. M. A. Sani and F. Separovic, *Acc Chem Res*, 2016, **49**, 1130-1138.
40. W. C. Wimley, *ACS Chem Biol*, 2010, **5**, 905-917.
41. S. Y. Kim, A. N. Bondar, W. C. Wimley and K. Hristova, *Biophys J*, 2021, **120**, 618-630.
42. K. Matsuzaki, S. Yoneyama and K. Miyajima, *Biophys J*, 1997, **73**, 831-838.
43. S. Y. Kim, A. E. Pittman, E. Zapata-Mercado, G. M. King, W. C. Wimley and K. Hristova, *J Am Chem Soc*, 2019, **141**, 6706-6718.
44. L. Sercombe, T. Veerati, F. Moheimani, S. Y. Wu, A. K. Sood and S. Hua, *Front Pharmacol*, 2015, **6**, 286.
45. F. Wang, R. M. Kream and G. B. Stefano, *Med Sci Monit*, 2020, **26**, e924700.
46. H. L. Huang, P. H. Lu, H. C. Yang, G. D. Lee, H. R. Li and K. C. Liao, *Int J Nanomedicine*, 2015, **10**, 5171-5184.
47. A. S. Ulrich, *Biosci Rep*, 2002, **22**, 129-150.
48. P. Milla, F. Dosio and L. Cattell, *Curr Drug Metab*, 2012, **13**, 105-119.
49. K. Hamamoto, Y. Kida, Y. Zhang, T. Shimizu and K. Kuwano, *Microbiol Immunol*, 2002, **46**, 741-749.